Original Article

MOLECULAR METABOLISM

Brown adipose Vanin-1 is required for the maintenance of mitochondrial homeostasis and prevents diet-induced metabolic dysfunction

Chen Sun[1,4], Jiaqi Liang[2,4], Jia Zheng[2], Shuyu Mao[2], Siyu Chen[2], Ainiwaer Aikemu[3,**], Chang Liu[2,*]

ABSTRACT

Background: Energy-dissipating brown adipocytes have significant potential for improving systemic metabolism. Vanin-1, a membrane-bound pantetheinase, is involved in various biological processes in mice. However, its role in BAT mitochondrial function is still unclear. In this study, we aimed to elucidate the impact of Vanin-1 on BAT function and contribution during overnutrition-induced obesity.

Methods: Vanin-1 expression was analyzed in different adipose depots in mice. The cellular localization of Vanin-1 was analyzed by confocal microscopy and western blots. Mice lacking Vanin-1 (Vanin-1$^{-/-}$) were continuously fed either a chow diet or a high-fat diet (HFD) to establish an obesity model. RNA-seq analysis was performed to identify the molecular changes associated with Vanin-1 deficiency during obesity. BAT-specific Vanin-1 overexpression mice were established to determine the effects of Vanin-1 in vivo. Cysteamine treatment was used to examine the effect of enzymatic reaction products of Vanin-1 on BAT mitochondria function in Vanin-1$^{-/-}$ mice.

Results: The results indicate that the expression of Vanin-1 is reduced in BAT from both diet-induced and leptin-deficient obese mice. Study on the subcellular location of Vanin-1 shows that it has a mitochondrial localization. Vanin-1 deficiency results in increased adiposity, BAT dysfunction, aberrant mitochondrial structure, and promotes HFD induced-BAT whitening. This is attributed to the impairment of the electron transport chain (ETC) in mitochondria due to Vanin-1 deficiency, resulting in reduced mitochondrial respiration. Overexpression of Vanin-1 significantly enhances energy expenditure and thermogenesis in BAT, renders mice resistant to diet-induced obesity. Furthermore, treatment with cysteamine rescue the mitochondrial dysfunction in Vanin-1$^{-/-}$ mice.

Conclusions: Collectively, these findings suggest that Vanin-1 plays a crucial role in promoting mitochondrial respiration to counteract diet-induced obesity, making it a potential therapeutic target for obesity.

Keywords Vanin-1; Diet-induced obesity; BAT; Mitochondrial thermogenesis; Electron transport chain

1. INTRODUCTION

Obesity is a multifactorial disease with metabolic alterations, typically manifested by hypertrophic adipocytes, increased inflammatory response and ectopic accumulation of harmful lipids in multiple tissues, and is associated with an increased risk of several diseases and conditions associated with increased mortality [1]. These include Type 2 diabetes mellitus (T2DM), cardiovascular diseases (CVD), metabolic syndrome (MetS), chronic kidney disease (CKD), hyperlipidemia, hypertension, nonalcoholic fatty liver disease (NAFLD), certain types of cancer, obstructive sleep apnea, osteoarthritis, and depression [2]. Metabolically, the main driver of obesity is an energy imbalance resulting from excessive energy intake relative to inadequate energy consumption [3]. While it is commonly believed that a balanced diet and exercise can effectively treat obesity, many individuals struggle to achieve this through self-control alone. Therefore, the use of medications plays a crucial role in obesity treatment. Currently, the main approach to treating obesity involves controlling energy intake, but this alone is insufficient to address the widespread prevalence of this epidemic due to the numerous adverse effects [4]. As a result, there has been a recent surge in research focusing on increasing energy expenditure as a means to combat obesity.

White adipose tissue (WAT) plays a crucial role in storing energy and regulating metabolic homeostasis [5]. However, it does not contribute significantly to energy expenditure. Numerous animal studies suggest that browning of WAT could have positive effects on overall energy

[1]School of Basic Medicine, Weifang Medical University, Weifang, Shandong 261000, China [2]State Key Laboratory of Natural Medicines and School of Life Science and Technology, China Pharmaceutical University, Nanjing 211198, China [3]Xinjiang Key Laboratory of Modernization Research, Development and Application of Hotan Characteristic Traditional Chinese Medicine Resources, College of Xinjiang Uyghur Medicine, Hotan 848099, China

[4] Chen Sun and Jiaqi Liang contributed equally to this work.

*Corresponding author. E-mail: changliu@cpu.edu.cn (C. Liu).

**Corresponding author. Xinjiang Key Laboratory of Hotan Characteristic Chinese Traditional Medicine Research, College of Xinjiang Uyghur Medicine, Hotan 848000, China E-mail: ainiwa@sina.com (A. Aikemu).

Received October 26, 2023 • Revision received January 6, 2024 • Accepted January 11, 2024 • Available online 19 January 2024

https://doi.org/10.1016/j.molmet.2024.101884

metabolism, but little is known about the browning susceptibility of human WAT [6]. On the other hand, brown adipose tissue (BAT) plays a vital role in energy expenditure through adaptive thermogenesis via mitochondria, contributing to the body's energy balance and maintenance of body temperature [7,8]. The discovery of BAT in adults has led to the exploration of activating or recruiting human brown fat as a potential treatment strategy for obesity, metabolic syndrome, and T2DM [9–11]. Brown adipocytes burn fat through uncoupling protein 1 (UCP1)-dependent uncoupling of mitochondrial oxidative phosphorylation (OXPHOS), which is supported by the coordination between substrate supply, mitochondrial oxidative machinery, and effectors controlling substrate oxidation rate [12,13]. Additionally, there are UCP1-independent modes involving energy-consuming futile cycles such as creatine cycling, calcium cycling, and the triglyceride (TG)/free fatty acid (FFA) cycle [14,15]. These pathways provide adipocytes with a significant thermogenesis capacity.

During thermoneutral adaptation and aging, BAT lose their normal structure and metabolic function, commonly referred to as 'whitening' of BAT [16]. With the progression of whitening, BAT acquires a white appearance, low UCP-1 expression, and mitochondrial dysfunction as featured by altered oxidative function, ultrastructure abnormalities, and increased oxidative stress [17]. Notably, previous studies have emphasized the significance of sufficient vasculature in improving mitochondrial function in BAT and reducing obesity-related complications [18,19]. Recently, BAT whitening has been defined as a long-term obesity complication that gradually worsens upon chronic intake of HFD [20,21]. Thus, with the rapidly rising prevalence of obesity, understanding the causative and underlying factors driving BAT whitening might help identify novel pharmacological targets to preserve or regain BAT metabolic capacity in humans.

Vascular non-inflammatory molecule 1 (Vanin-1), a glycosylphosphatidylinositol (GPI)-anchored pantetheinase, recycles pantothenic acid (also known as vitamin B5) by hydrolyzing pantetheine, which is an important molecular framework for coenzyme A (CoA) biosynthesis [22]. Therefore, Vanin-1 has high expression levels in tissues with high CoA conversion rates, such as lung, liver, kidney, gastrointestinal tract, spleen, blood, and skin in humans and rodents [23]. Cysteamine, another metabolite resulting from the reaction, is known for its antioxidant potential in vitro and is used in the treatment of cystinosis [24,25]. At low concentrations, cysteamine affects the transport of cysteine and the metabolism of glutathione [26,27]. When cysteamine is added to cultured cells, it increases the uptake of cysteine and the synthesis of GSH. Conversely, high concentrations of cystamine, the oxidized form of cysteamine, inhibit γ-glutamylcysteine synthetase, depleting the intracellular stores of GSH [28]. Together, cysteamine and cystamine contribute to the regulation of intracellular redox homeostasis through protein disulfide bond exchange. As a result, Vanin-1 is considered an important sensor of oxidative stress. Vanin-1 is the prototypic member of a larger family containing three genes in man (VNN1, VNN2, VNN3), two in mouse (Vanin-1, Vanin-3) [29]. VNN2 is primarily distributed on human neutrophils and monocytes, and is stored in secretory vesicles as an intracellular reservoir. Studies have shown that VNN2 plays a role in regulating β2 integrin-mediated cell adhesion, cell migration, and motility of neutrophils [23]. The dysregulated Vanins played significant roles of biomarkers in disease diagnosis and prognosis. Various studies have emphasized the role of Vanin-1 in the etiology and pathogenesis of metabolic disorders [22]. It was previously demonstrated that Vanin-1 prevented the development of fasting-induced hepatic steatosis in mice [30]. Our previous research has also demonstrated that Vanin-1 plays a crucial role in activating hepatic gluconeogenesis and WAT lipolysis [31,32]. Recent work shows that exogenous expression of Vanin-1 restores the content of CoA and enhance the mitochondrial activity of tumor cells under Warburg effect [33]. During the progression of BAT whitening, Brown adipocytes undergoes a process of oxidative stress and inflammation, causing mitochondrial dysfunction. We hypothesized that Vanin-1 is the key regulator to maintain BAT mitochondrial homeostasis, and the intervention of Vanin-1 is expected to be an effective measure to reverse the "whitening" of BAT.

Herein, we explored the role of Vanin-1 in BAT thermogenesis and the conversion of brown adipocytes to white-like adipocytes in obesity. Our findings showed a decrease in the expression of Vanin-1 in BAT of obese mice. Interestingly, we discovered that Vanin-1 is not only present on the cell surface of brown adipocytes but also within mitochondria. Vanin-1 deficiency exacerbates HFD-induced BAT whitening and obesity in mice. Additionally, we observed that Vanin-1 knockout hindered energy expenditure and mitochondrial thermogenesis in BAT of HFD mice. However, the overexpression of Vanin-1 specifically in BAT improved the whitening phenotype in HFD mice, leading to increased mitochondrial contents and UCP1 expression. Furthermore, these mice exhibited reduced fat mass and improved insulin tolerance. Mechanistically, Vanin-1 induced the expression of genes involved in mitochondrial electron transport chain (ETC) and thermogenesis in BAT. Importantly, we found that the mitochondrial dysfunction observed in BAT of Vanin-1$^{-/-}$ mice could be effectively reversed by restoring cysteamine. In conclusion, our study highlights the crucial role of Vanin-1 in maintaining mitochondrial homeostasis in BAT. Furthermore, we report for the first time that Vanin-1 localizes within mitochondria in brown adipocytes, which is an unusual subcellular localization.

2. MATERIALS AND METHODS

2.1. Animal models and treatment

All studies involving animal experimentation in this investigation conform to the Guide for the Care and Use of Laboratory Animals published by the US National Institutes of Health (NIH publication No. 85-23, revised 1996) and the approved regulations set by the Laboratory Animal Care Committee at China Pharmaceutical University (Permit number SYXK-2016-0011). Mice were maintained in a 12 h light–dark cycle and housed at thermoneutral (26–28 °C) temperature- and humidity-controlled environment, and with ad libitum access to food and water. Male C57BL/6J and genetically obese C57BL/6J ob/ob mice were purchased from GemPharmatech Co., Ltd (Nanjing, Jiangsu, China). Vanin-1$^{-/-}$ mice with the C57BL/6J genetic background were kindly provided by Prof. Franck Galland (CIML, INSERM-CNRS, France) and genotyped as described previously [29]. For HFD-feeding experiments, mice were fed a chow diet or HFD (60 % calories from fat). For Vanin-1 overexpression, 50 μL (1 × 10^{10} vector genomes (VG) per mouse) AAV8-CMV-Vanin-1 (vector carrying unmodified coding sequence of mouse Vanin-1 (NCBI Reference Sequence: NM_011704.3)) or negative control AAV8-CMV-GFP was injected into interscapular BAT of overexpressed mice and control group, respectively.

Mice were anesthetized by isoflurane. Lateral skin incisions were made around the area of the interscapular BAT. AAV was injected at multiple sites into fat pads (5–8 spots per fat pad). For cysteamine treatment, Vanin-1$^{-/-}$ mice were administrated with cysteamine (150 mg/kg/day) in drinking water and provided *ad libitum* access as well for 4 weeks [34].

2.2. Murine brown adipocyte culture

Primary brown preadipocytes were isolated from the interscapular BAT of the mouse according to the methods described previously

[35], and cultured in Dulbecco's Modified Eagle's Medium (DMEM) (Gibco) supplemented with 10 % fetal bovine serum (FBS, Sciencell Research, Carlsbad, CA, USA). For differentiation assays, mouse primary brown preadipocytes were grown to confluence and then switch to differentiation medium (DMEM with 10 % FBS, 1 μM dexamethasone, 0.5 mM 3-isobutyl-1-methylxanthine (IBMX), 125 nM indomethacin, 20 nM insulin and 1 nM T3). The cells were subsequently maintained in above medium for 2 days. The cells were then cultured in fresh medium supplemented with 20 nM insulin and 1 nM T3 for up to 4 days, and the medium was replaced every other day. Then, brown adipocytes were cultured in DMEM with 10 % FBS until they were treated for experiments. All cells were cultured and maintained at 37 °C in a 5 % CO2 incubator. The medium was supplemented with 1 % penicillin and 1 % streptomycin (Invitrogen).

2.3. RNA extraction and reverse transcription-quantitative PCR (RT-qPCR)

Total RNA was extracted using TRIzol reagent (Invitrogen, Carlsbad, CA, USA), reverse transcribed to complementary DNA (cDNA) by using Hiscript® II Q RT SuperMix for qPCR Kit (Vazyme, Nanjing, Jiangsu, China), and analyzed by qPCR using SYBR Green (Vazyme, Nanjing, Jiangsu, China) and the LightCycler® 480 System (Roche, Basal, Switzerland). The primers for mouse β-Actin were included for normalization. A complete list of primers for RT-qPCR is shown in Table S1.

2.4. Western blot analysis

Homogenized tissues or cultured cells were lysed in RIPA buffer. The protein concentration was quantified by using the Enhanced BCA Protein Assay Kit (Beyotime, Shanghai, China). Equal amounts of protein were loaded and separated by SDS-PAGE, and then transferred onto polyvinylidene difluoride membranes (Millipore, Bedford, MA, USA). The protein of interest was visualized by using appropriate primary antibodies and HRP-conjugated secondary antibodies. Quantification of Western blot was done using AlphaEaseFC software (Alphalnnotech, San Leando, CA, USA), and the grayscale values of target proteins were normalized to that of the β-Actin on the same membrane.

2.5. Detection of mice metabolic rate

After 4 weeks of AAV injection, mice were fed with HFD for 10 weeks. Mice were acclimatized in a metabolic chamber for 24 h prior to measurement of metabolic parameters. Energy expenditure was assessed using Phenomaster automated modular system (TSE Systems GmbH, Germany). The concentrations of VO_2 and VCO_2 were monitored at the inlet and outlet of the sealed chambers to calculate O_2 consumption and CO_2 production.

2.6. Body temperature measurements

During experiments on cold exposure, mice were placed in cages prechilled to 4 °C and provided with unrestricted access to food and water. The rectal temperature was recorded at specified intervals following cold stimulation using an animal electronic thermometer.

2.7. Glucose and insulin tolerance tests

In the glucose tolerance test (GTT), mice were fasted for 16 h and then intraperitoneally injected with glucose (1 g/kg body weight). In the insulin tolerance test (ITT), mice were fasted for 6 h and intraperitoneally injected with insulin (2 U/kg body weight). Blood glucose levels were recorded before the injection and 15, 30, 60, 120 min after the injection by a glucose monitor (Roche Diagnostics, Indianapolis, IN, USA). Areas under curve were calculated and statistically analyzed by using GraphPad Prism 8.0.1. (Graph Pad Software, San Diego, CA, USA).

2.8. Tissue lipid analysis

Liver tissues (50 mg per sample) were homogenized, TG and TC contents were measured by using commercial kits (Jiancheng Institute of Biotechnology, Nanjing, Jiangsu, China) according to the manufacturer's instructions and normalized by total protein amount.

2.9. Serological analysis

Blood samples were collected in nonheparinized tubes and centrifuged at 4 °C for 10 min at 4000 rpm. Serum TG and TC were determined by using commercial kits (Jiancheng Institute of Biotechnology, Nanjing, Jiangsu, China) according to manufacturer's instructions.

2.10. Histological staining

Fresh BAT, sWAT, eWAT and liver tissues were fixed with 4 % paraformaldehyde solution for 24 h. For hematoxylin—eosin (H&E) staining, samples were embedded in paraffin, continuously cut into 5 mm sections and stained with hematoxylin/eosin following standard protocols. Average adipocytes size was calculated with NIH Image J 1.32j software (NIH, Bethesda, MD, USA). For immunohistochemistry (IHC) staining, paraffin-embedded tissue slides were deparaffinised and antigen retrieved in citric acid buffer, blocked in 5 % normal goat serum, and incubated with antibodies: anti-Vanin-1 (Cat. No. 21745-1-AP; 1:100 dilution, Proteintech, Wuhan, China) or anti-UCP1 (Cat. No. 23673-1-AP; 1:100 dilution, Proteintech, Wuhan, China) at 4 °C overnight. After washing, the slides were incubated with the secondary antibodies. Diaminobenzidine was used for target protein visualization. Images were taken by a Nikon microscope (400× magnification, ECLIPSE, Ts2R-FL, Tokyo, Japan).

2.11. RNA sequencing

Microarray was performed to identify differentially expressed genes (DEGs) in BAT between the WT and Vanin-$1^{-/-}$ mice fed with HFD. Total RNA was isolated from BAT using TRIzol (Invitrogen). Library sequencing and data analysis were performed on a HiSeq 3000 sequencing platform (Illumina Company, USA) by APTBIO Co. Ltd (Shanghai, China).

2.12. Detection of mtDNA content

Total DNA was extracted from BAT for the quantitation of mtDNA copy number by using Dneasy Blood & Tissue Kit (QIAGEN, Shanghai, China). RT-qPCR was performed using nuclear DNA primers (*Tert*) and mtDNA primer (mtDNA loop1). The *Tert* DNA values served to normalize the mtDNA values. The sequences of primers are listed in Table S1.

2.13. Oil Red O staining

For in vitro analysis, fully differentiated primary brown adipocytes were washed with PBS and fixed with 4 % paraformaldehyde, followed by incubation in Oil Red O staining solution. Stained cells were rinsed in 60 % isopropanol to remove excess Oil Red O staining solution. For in vivo analysis, OCT-embedded frozen liver sections were cut into 5 μm sections and stained with Oil Red O to visualize steatosis. Images of red lipid droplets were taken by a Nikon microscope (400× magnification, ECLIPSE, Ts2R-FL, Tokyo, Japan).

2.14. Mito-Tracker Red staining

Cultured cells were incubated in DMEM with Mito-Tracker Red (Beyotime Biotechnology) for 20 min in a 37 °C incubator and then

rinsed two times in PBS. Cell nuclei were labeled with Hoechest 33342 (Sigma—Aldrich). Images were taken by a Nikon microscope (400× magnification, ECLIPSE, Ts2R-FL, Tokyo, Japan).

2.15. Immunofluorescence

Fully differentiated primary brown adipocytes were fixed with 4 % paraformaldehyde for 30 min, permeabilized with 0.2 % Triton X-100 for 10 min, and blocked with 5 % bovine serum albumin (BSA) for 60 min. Cells were incubated with primary antibody at 4 °C overnight and incubated with the corresponding secondary antibody for 1 h at 37 °C. Cell nuclei were labeled with diamidino-2-phenylindole (DAPI) (Thermo Fisher Scientific) at room temperature for 5 min. Images were acquired with a confocal laser scanning microscope (CLSM, LSM700, Zeiss, Germany) and processed using the ZEN imaging software.

2.16. Isolation of mitochondria

Mitochondria were isolated from BAT by using Cell Mitochondria Isolation Kit (Beyotime, Shanghai, China) according to the manufacturer's protocol.

2.17. Transmission electron microscopy (TEM)

BAT was isolated from the mice and immediately cut into small pieces (1 μm × 1 μm × 1 μm) in ice-cold PBS. Samples were gently shaken in buffer (2.5 % glutaraldehyde and 2 % paraformaldehyde [pH 7.4] in 0.1M sodium cacodylate) incubated at 4 °C for 24 h. Subsequent processing was carried out by the Shiyanjia Lab (www.shiyanjia.com). TEM was performed with a JEM-2100F at 80 kV, and a side-inserted BioScan camera was for acquired photos.

2.18. Assessment of oxygen consumption assay

Oxygen consumption rate (OCR) was assessed by a Seahorse XF24 extracellular flux analyzer (Agilent, Santa Clara, CA, USA). Primary brown preadipocytes isolated from BAT were seeded into each well of gelatin-coated 24-well seahorse cell culture plates and differentiated into mature brown adipocytes. Fully differentiated primary brown adipocytes were rinsed twice and then cultured in Agilent Seahorse XF Base Medium containing 25 mM glucose and 1 mM pyruvate for 1 h in a non-CO2 incubator at 37 °C. Plates were then transferred to a Seahorse XF24 analyzer for mitochondrial stress testing. OCR was measured under basal condition and upon sequential addition of different reagents. Oligomycin (1 μM), a coupled respiration inhibitor, was added for assessment of ATP production and proton leak. Carbonyl cyanide-4-(trifluoromethoxy) phenylhydrazone (FCCP) (600 nM) was added for assessment of the maximal respiration of the cells. Rotenone (0.5 μM) and antimycin A (0.5 μM) were added for assessment of the non-mitochondrial respiration of the cells.

2.19. GC—MS (gaschromatography—mass spectrometry)

2.19.1. Internal standard configuration

0.66 g of cysteamine standard was accurately weighed and added to 20 ml of purified water to prepare a 4.4 μmol/L standard.

2.19.2. Derivatization

50 μL of IsoBCF and 200 μL of NaOH were added to 800 μL of mouse serum and shaken at 300 rpm at room temperature for 5 min. The mixture was extracted with 800 μL of ethyl acetate and the extract was evaporated to dryness at 45 °C. The residue was dissolved in 80 μL of ethyl acetate and transferred to a sample vial for GC/MS analysis.

2.19.3. Gas chromatographic conditions

TG-5 MS Column {30 m × 0.25 mm × 0.25 μm, 5 % cyanopropylphenyl and 95 % dimersiloxane stationary solution}; The inlet temperature was 280 °C, the program temperature was increased to 50 °C for 1 min, then increased to 100 °C at a rate of 5 °C/min, and finally increased to 280 °C at a rate of 20 °C/min for 4 min. The carrier gas is high-purity helium with a flow rate of 1 mL/min. The collision gas is high-purity nitrogen; the injection method is splitless injection; the injection volume was 1.0 μL.

2.19.4. Mass spectrometry conditions

The ionization method is EI: the ion source temperature is 230 °C, and the transmission line temperature is 280 °C. The four-stage rod temperature is 150 °C. The solvent delay was 5.0 min; Select the Ion Monitoring Mode (SIM). The quantification ion of the sample was determined to be m/z 144. The external standard method was used to quantitatively detect the pyrolysis gas components.

2.20. Statistical analyses

All data are presented as mean ± SEM. Statistical analysis was performed by using Graphpad Prism 8 (GraphPad, San Diego, CA). The unpaired Student *t*-test (two-tailed) was performed to analyze the data. A value of $p < 0.05$ was considered as statistically significant. N.S.: not significant ($p > 0.05$).

3. RESULTS

3.1. Vanin-1 expression is decreased in BAT of obese mice

To investigate the physiological function of Vanin-1 in BAT, we initially examined its protein levels in different fat depots of C57BL/6J mice. Figure 1A demonstrates a strong expression of UCP1 in BAT, which is consistent with previous studies. Similarly, Vanin-1 showed higher expression in interscapular BAT compared to subcutaneous WAT (sWAT) and visceral epididymal WAT (eWAT). Unlike white adipocytes, brown adipocyte mitochondria appear to be more numerous and larger, with densely packed cristae. These mitochondria play a central role in providing the energy required for thermogenesis in BAT. Despite being annotated as a cell-surface and secreted pantetheinase without a discernible mitochondrial targeting sequence (UniProt: Q9Z0K8), Figure 1B demonstrates the presence of Vanin-1 in mitochondrial preparations from BAT. Subsequently, we investigated the intracellular distribution of Vanin-1 using immunocytochemistry and observed a significant amount of Vanin-1 co-localizing with the well-known mitochondrial protein HSP60. (Figure 1C). Moreover, we examined the localization of Vanin-1 in hepatocytes and found that the mitochondrial localization was present (Fig. S1E).

Previous studies have indicated that obese animals and humans often exhibit a whitened phenotype in BAT, which is associated with decreased BAT activity and complications such as insulin resistance. In order to further investigate the relationship between obesity and BAT function, we examined Vanin-1 expression levels in two mouse models of obesity: HFD-induced obese mice and leptin (ob/ob)-deficient mice. Our RT-qPCR analysis (Figure 1D) revealed a significant suppression of Vanin-1 mRNA expression in BAT of HFD-treated mice. This was further supported by our Western blot and immunohistochemistry (IHC) analyses, which showed lower levels of Vanin-1 protein in BAT of HFD-treated mice (Figure 1E, F, Fig. S1A and S1B). Similar patterns were observed in the expression of Vanin-1 in BAT of ob/ob mice, at both the transcriptional and translational levels (Figure 1G—I, Fig. S1C and S1D). Notably, the downregulation of Vanin-1 expression was accompanied by a decrease in UCP1 expression in BAT of both ob/ob and HFD-

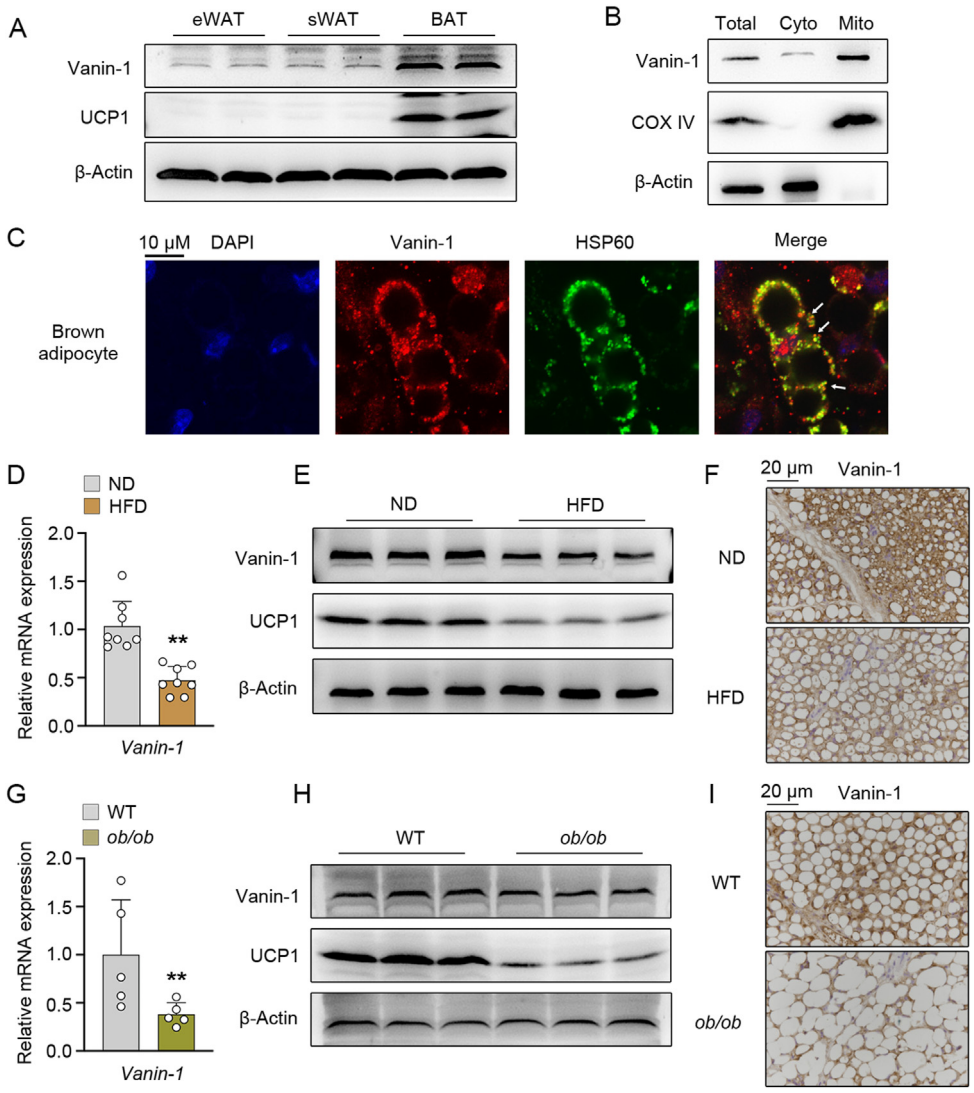

Figure 1: Vanin-1 is highly expressed in BAT, appears irregularly in mitochondria, and shows reduced expression in BAT of obese mice. (A) Representative western blots of Vanin-1 and UCP1 protein expression in the epididymal white (eWAT), subcutaneous white (sWAT), and brown adipose tissue (BAT) of mice. $n = 6$ (B) Representative western blots of Cytoplasmic (Cyto) and mitochondrial (Mito) Vanin-1 and COX IV protein expression in BAT of mice. (C) Confocal fluorescence images showing the subcellular localization of ectopically expressed Vanin-1 in immortalized brown adipocytes. Anti-Vanin-1 (red) and and anti-HSP60 (green) were used to visualize Vanin-1 and mitochondria, respectively. White arrows denote Vanin-1 signals that co-localize with mitochondrial marker HSP60. (D–F) Mice were fed with either a normal diet (ND) or an HFD for 16 weeks. (D) RT-qPCR analysis of Vanin-1 mRNA expression in BAT. ($n = 8$). (E) Representative western blot analysis of Vanin-1 and UCP1 protein expression in the BAT ($n = 9$). (F) IHC staining of Vanin-1 expression in the BAT ($n = 3$). (G–I) Twelve-week- old WT and ob/ob mice fed ad libitum. (G) RT-qPCR analysis of Vanin-1 mRNA expression in the BAT from WT or ob/ob mice. ($n = 5$). (H) Representative Western blot analysis of Vanin-1 and UCP1 protein expression in the BAT from WT or ob/ob mice ($n = 5$). (I) IHC staining of Vanin-1 expression in the BAT from WT or ob/ob mice ($n = 3$). For statistical analysis, unpaired two-tailed Student's t tests were performed in (D) and (G). $^{**}p < 0.01$. All values are presented as the mean ± SD.

induced obese mice. These findings suggest a positive correlation between Vanin-1 expression and UCP1 expression, and also indicate that reduced Vanin-1 expression may contribute to the whitening of BAT and impair systemic energy homeostasis. In addition, we also found that Vanin-3, another member of the pantetheinase family, has reduced expression in brown adipose in obese mice (Fig. S1F and S1G).

3.2. Vanin-1 deficiency predisposes HFD-fed mice to BAT whitening

To investigate the role of Vanin-1 in BAT Whitening, we performed experiments with whole-body Vanin-1$^{-/-}$ mice fed ad libitum and identified their phenotypes (Fig. S2A). We observed an increase in body weight in 13-week-old mice under normal diet (ND) (Fig. S2B), along with a noticeable increase in the weight of interscapular BAT (Fig. S2C and S2D). Hematoxylin and eosin staining revealed a higher proportion of large adipocytes in the interscapular BAT (Fig. S2E and S2F), indicating brown adipocyte hypertrophy in Vanin-1$^{-/-}$ mice. We then examined the expression of brown and white adipocyte marker genes to confirm the whitening character of BAT. The mRNA expression of BAT marker genes, including *Ucp1*, *Pgc-1a*, Cidea and *Dio2*, was significantly decreased in BAT of Vanin-1$^{-/-}$ mice (Fig. S2G). However, *Prdm16* mRNA expression was not changed (Fig. S2G). Moreover, we did not observe any significant difference in the mRNA expression levels of *Rb1* and *Nrip1*, which inhibit BAT differentiation, in

BAT of Vanin-1$^{-/-}$ mice (Fig. S2H). Similarly, there was no change in the expression of *Adipoq* (WAT marker gene) (Fig. S2H). Furthermore, the protein levels of UCP1 and Prdm16 were significantly reduced (Fig. S2I and S2J). These results suggest that Vanin-1 deletion did not directly cause the whitening of BAT, but rather attenuated its function. However, with HFD for 8 weeks at 8 weeks of age, Vanin-1$^{-/-}$ mice exhibited a significant increase in body weight compared to WT mice (Figure 2A). Importantly, there was no significant difference in food intake between the two groups of mice (Figure 2B). Moreover, the interscapular BAT from HFD-fed Vanin-1$^{-/-}$ mice was larger and heavier than that in the HFD-fed WT mice (Figure 2C,D). Histological analysis revealed a significant increase in the size of large adipocytes in the BAT (Figure 2E,F). Furthermore, the serum level of total cholesterol (TC) was upregulated, while no difference in the serum content of triglyceride (TG) was observed between these two HFD-treated genotypes (Figure 2G,H). Consistent with these observations, the mRNA expression levels of BAT differentiation marker genes (e.g., *Ucp1, Prdm16, Pgc-1a, Cidea* and *Dio2*) were similarly reduced in BAT from Vanin-1$^{-/-}$ mice (Figure 2I). Additionally, both BAT differentiation inhibition-related genes (*Rb1* and *Nrip1*) and WAT marker gene (*Adipoq*) were elevated at the mRNA level in BAT from Vanin-1$^{-/-}$ mice (Figure 2J). The protein expression levels of UCP1 and Prdm16 exhibited a similar pattern, as assessed by Western blot and IHC analyses (Figure 2E, K and Fig. S2L). These findings indicate that the loss of Vanin-1 facilitates HFD-induced BAT whitening.

To investigate the impact of Vanin-1 on brown adipocytes differentiation, we conducted in vitro experiments. Our findings revealed a gradual increase in Vanin-1 expression during the differentiation of mouse primary brown adipocytes (Fig. S3A and S3B). The staining with Oil red O (ORO) (Fig. S3C) and BODIPY (Fig. S3D) indicated that reduction of lipid droplets was more pronounced in Vanin-1$^{-/-}$ brown adipocytes compared to WT cells. Additionally, the expression levels of BAT marker genes were lower in Vanin-1$^{-/-}$ brown adipocytes (Fig. S3E), suggesting that Vanin-1 deficiency leads to a reduction in brown adipocyte differentiation.

3.3. Vanin-1 deficiency leads to the decrease and dysfunction of mitochondrial in BAT

To further study the mechanism by which Vanin-1 deficiency aggravates the whitening of BAT, we conducted gene sequencing of BAT in HFD-treated WT and Vanin-1$^{-/-}$ mice. A total of 4700 genes exhibited more than a 2-fold expression levels change in the BAT of Vanin-1$^{-/-}$

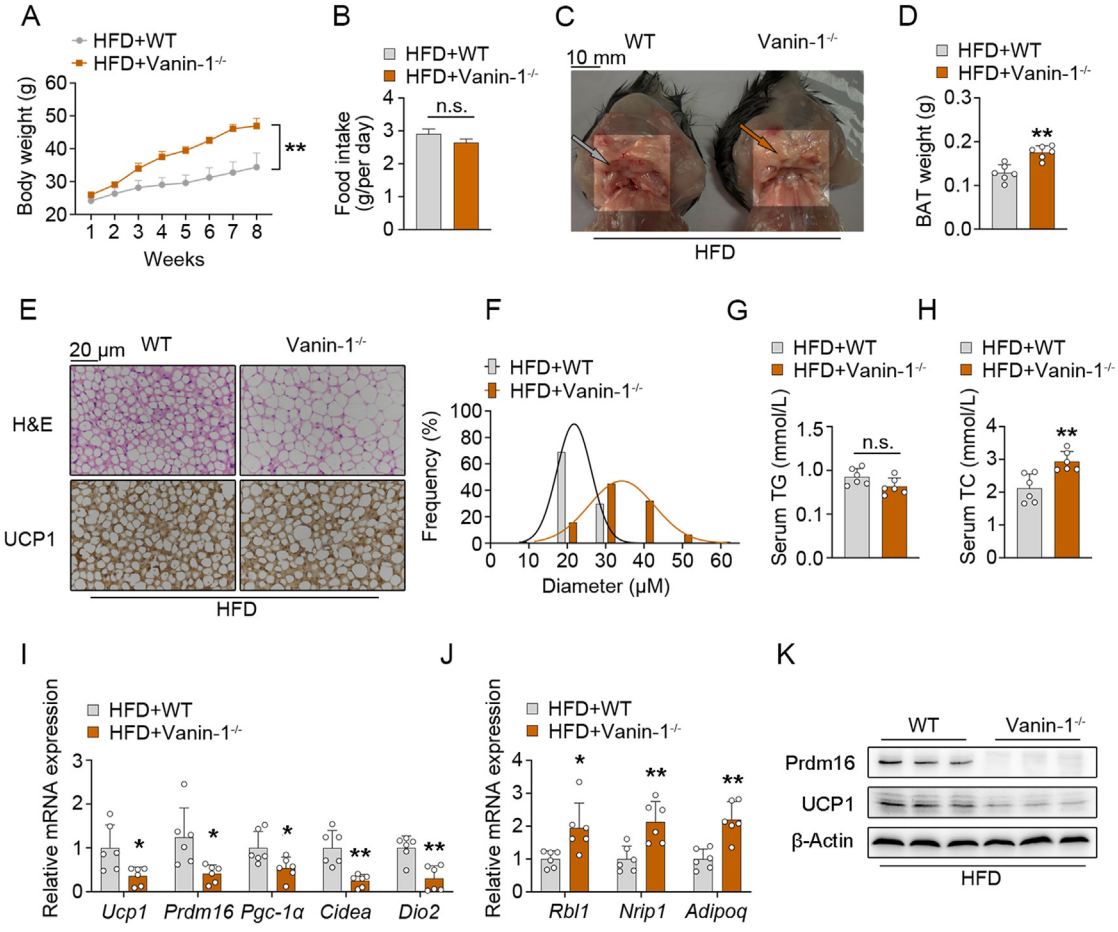

Figure 2: Vanin-1 deficiency aggravates HFD-induced BAT whitening in mice. (A) The growth curve of WT and Vanin-1$^{-/-}$ mice on HFD for 8 weeks ($n = 6$). (B) Daily food intake of WT and Vanin-1$^{-/-}$ mice on HFD for 8 weeks ($n = 6$). (C) Representative images of BAT from WT or Vanin-1$^{-/-}$ mice on HFD for 8 weeks. (D) The weight of BAT from the mice in (C) ($n = 6$). (E) Representative images of H&E staining (upper) and IHC staining of UCP1 (lower) in BAT from the mice in (C). Scale bar, 20 μm. (F) Distribution of brown adipocyte diameter (μm) in (E). (G and H) Serum TG (G) and TC (H) levels in WT and Vanin-1$^{-/-}$ mice on HFD for 8 weeks ($n = 6$). (I and J) RT-qPCR analysis of BAT marker genes (I) and WAT marker genes (J) in BAT of WT or Vanin-1$^{-/-}$ mice on HFD for 8 weeks ($n = 6$). (K) Representative Western blot analysis of Prdm16 and UCP1 protein expression in BAT from WT or Vanin-1$^{-/-}$ mice on HFD for 8 weeks. β-actin was used as a loading control. For statistical analysis, unpaired two-tailed Student's *t* tests were performed in (B), (D), (G), (H), (I), and (J). $^{*}p < 0.05$, $^{**}p < 0.01$. All values are presented as the mean ± SD.

mice compare to WT mice. The volcano plot demonstrated that 2765 genes were upregulated, while 1935 genes were downregulated (Figure 3A). Subsequent Kyoto Encyclopedia of Genes and Genomes-enriched (KEGG-enriched) pathway analysis indicated a significant downregulation of oxidative phosphorylation, thermogenesis, and the PI3K-Akt signaling pathway in Vanin-1$^{-/-}$ mice (Figure 3B). The electron transport chain (ETC), which consists of five protein complexes (C—I to C—V), plays a crucial role in mitochondrial respiration. Our microarray data confirmed a downward trend in ETC-related genes (Figure 3C), suggesting that Vanin-1 deficiency led to ETC defects in these mice. Therefore, we examined the mitochondrial ultrastructure of BAT from WT and Vanin-1$^{-/-}$ mice using transmission electron microscopy (TEM). In normal brown adipocytes, mitochondria displayed well-preserved membrane structures and neatly aligned crests. In stark contrast, mitochondria in Vanin-1$^{-/-}$ mice at 8 weeks of age displayed aberrant structure with disorganized cristae, along with a decrease in abundance (Figure 3D,E). Consistent with the reduced mitochondrial abundance, we also observed a significant reduction of mtDNA copy number in BAT from Vanin-1$^{-/-}$ mice (Figure 3F), suggesting that Vanin-1 deficiency in BAT leads to impaired mitochondrial integrity and mass. Furthermore, at the molecular level, we observed a dramatic decrease in mRNA and protein expression levels of ETC-related genes in the BAT of Vanin-1$^{-/-}$ mice (Figure 3G, H and Fig. S2K).

According to studies conducted on HFD-fed mice in the Vanin-1 deficient background, it has been found that Vanin-1 plays a significant role in regulating mitochondrial homeostasis. The absence of Vanin-1 reduces thermogenesis and oxidative phosphorylation in the BAT, which ultimately worsens the metabolic syndromes in HFD-fed mice.

3.4. BAT-specific Vanin-1 overexpression protects mice against HFD-induced metabolic dysfunction

To confirm the effects of Vanin-1 on mitochondrial homeostasis and whole-body metabolism, we utilized a gain-of-function strategy through adeno-associated virus (AAV)-mediated gene transfer. We specifically overexpressed Vanin-1 in the brown adipose tissue (BAT)

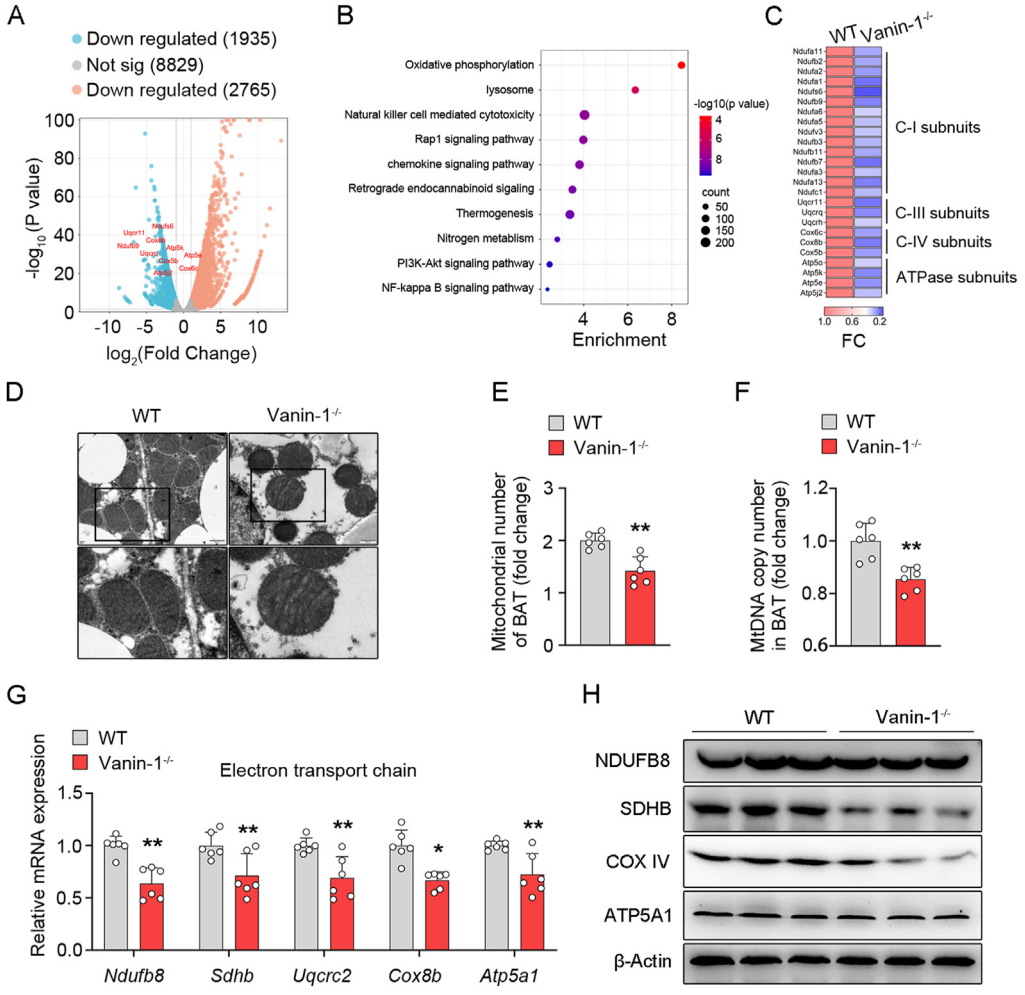

Figure 3: Mitochondrial in BAT from Vanin-1$^{-/-}$ mice show reduced oxidative phosphorylation and structure damage. (A) The volcano plot of RNA-seq showing up- and downregulated genes between WT and Vanin-1$^{-/-}$ mice. (B) Kyoto Encyclopedia of Genes and Genomes (KEGG) analysis of regulated pathway in WT and Vanin-1$^{-/-}$ mice. (C) Heatmap showing fold change of electron transport chain (ETC)-related genes mRNA levels in (A). (D and E) Mitochondrial structures of BAT from WT and Vanin-1$^{-/-}$ mice. (D) Representative electron microscopy (EM) images of BAT. Black boxes denote magnified areas. Scale bar, 1 μm. (E) Quantification of mitochondrial numbers. Six fields were randomly chosen for each group. (F) mtDNA copy number of BAT from WT and Vanin-1$^{-/-}$ mice ($n = 6$). (G) RT-qPCR analysis of ETC-related genes mRNA expression in BAT from WT or Vanin-1$^{-/-}$ mice ($n = 6$). (H) Representative Western blot analysis of ETC-related genes protein expression in BAT from WT or Vanin-1$^{-/-}$ mice. β-actin was used as a loading control. For statistical analysis, unpaired two-tailed Student's t tests were performed in (E), (F), and (G). $^{*}p < 0.05$, $^{**}p < 0.01$. All values are presented as the mean ± SD.

of mice by injecting AAV8-CMV-GFP or AAV8-CMV-Vanin-1 directly into the BAT (Figure 4A). The overexpression efficiency was validated in Fig. S4A of the Supporting Information, which showed a significant increase in Vanin-1 expression in the BAT of mice after intra-BAT AAV8-CMV-Vanin-1 injection. By contrast, Vanin-1 expression was no affected in other organs such as WAT and liver (Fig. S4B and S4C). Firstly, we investigated the thermogenic ability of AAV-GFP and AAV-Vanin-1 mice by subjecting them to 4 °C temperatures. Contrary to our hypothesis, after 6 h at 4 °C, the rectal temperature of AAV-Vanin-1 mice remained significantly higher than that of AAV-GFP mice (Figure 4B). To further illustrate the impact of Vanin-1 on obesity, we fed two groups of mice with HFD for 10 weeks. HFD-AAV-Vanin-1 mice exhibited slower weight gain compared to HFD-AAV-GFP mice (Figure 4C), despite no significant difference in daily food intake (Figure 4D). In addition, glucose tolerance test (GTT) (Figure 4E) and insulin tolerance test (ITT) (Figure 4F) results showed that HFD-AAV-Vanin-1 mice had a more efficient clearance of plasma glucose compared to HFD-AAV-GFP mice, as evidenced by the reduced area under the curve (AUC) of GTT (Fig. S4D) and increased inverse AUC of ITT (Fig. S4E), respectively. Furthermore, we measured daily O_2 consumption and energy expenditure (EE) in mice using metabolic cages. As shown in Figure 4G,H, our findings revealed that O_2 consumption was significantly higher in HFD-AAV-Vanin-1 mice during both the dark and light phases compared to HFD-AAV-GFP mice. Additionally, EE,

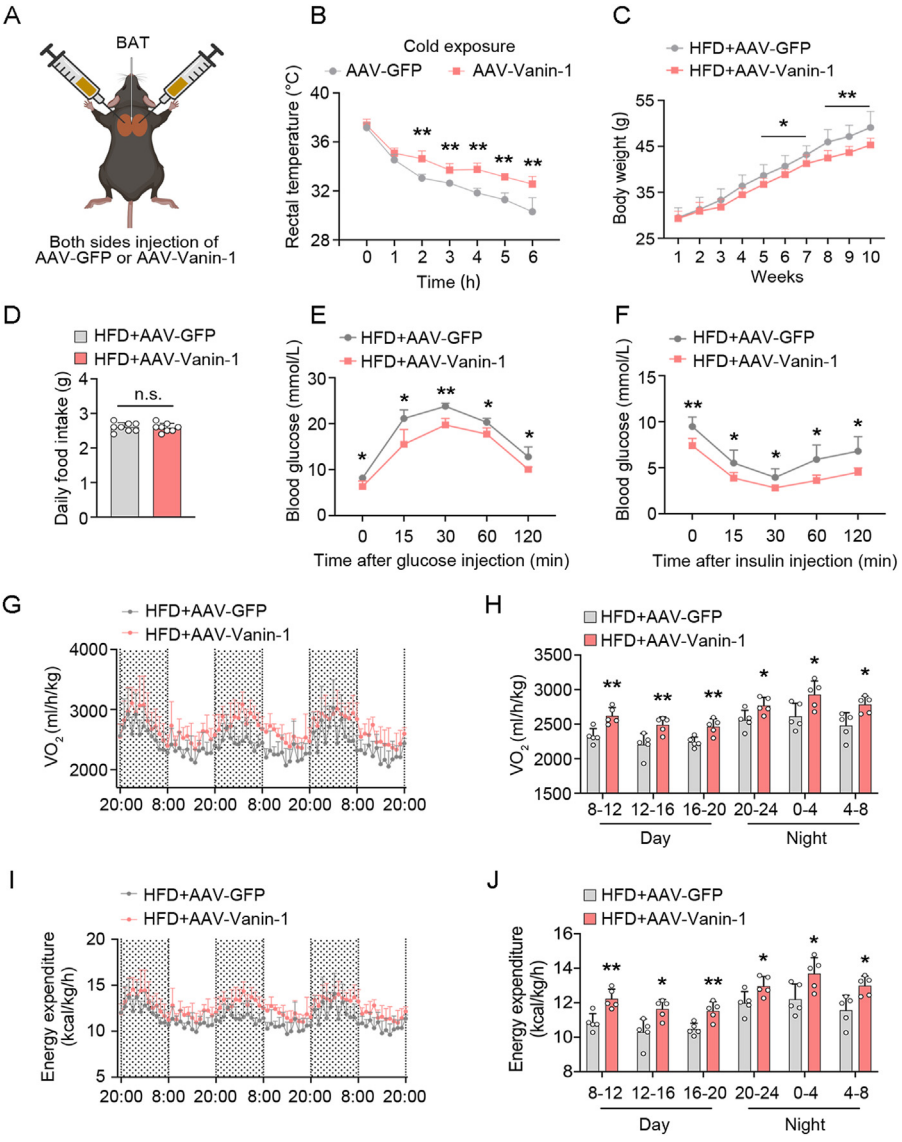

Figure 4: Vanin-1 overexpression in BAT enhance energy expenditure, improve glucose tolerance and insulin sensitivity in HFD mice. (A) Schematic representation showing AAV injection in BAT of mice. (B) The rectal temperature of 6-week-old mice injected with AAV-GFP or AAV-Vanin-1 during acute cold exposure (4 °C) ($n = 6$). AAV-GFP, adeno-associated vector expressing GFP; AAV-Vanin-1, deno-associated vector expressing Vanin-1. (C) Body weight of AAV-GFP or AAV-Vanin-1 injection mice fed on HFD. (D) Daily food intake of AAV-GFP or AAV-Vanin-1 injection mice fed on HFD ($n = 8$) (E) Glucose tolerance test (GTT) in AAV-GFP or AAV-Vanin-1 injection mice fed on HFD for 10 weeks ($n = 4$). (F) Insulin tolerance test (ITT) in AAV-GFP or AAV-Vanin-1 injection mice fed on HFD for 10 weeks ($n = 5$). (G and H) Oxygen consumption (VO2) was determined by metabolic cages in AAV-GFP or AAV-Vanin-1 injection mice fed on HFD for 10 weeks ($n = 5$). (I and J) Energy expenditure (EE) was estimated by amount of O2 consumption and CO2 production in AAV-GFP or AAV-Vanin-1 injection mice fed on HFD for 10 weeks ($n = 5$). For statistical analysis, unpaired two-tailed Student's *t* tests were performed in (B), (C), (D), (E), (F), (H), and (J). $*p < 0.05$, $**p < 0.01$. All values are presented as the mean ± SD.

estimated by the amount of O_2 consumption and CO_2 production during nutrient oxidation, was also significantly increased in HFD-AAV-Vanin-1 mice (Figure 4I,J). These results suggest that Vanin-1 overexpression enhances EE in HFD mice, independent of food intake. In summary, our data demonstrate that Vanin-1 overexpression in brown adipose tissue significantly enhances whole-body EE, indicating that HFD-AAV-Vanin-1 mice have greater energy utilization.

To assess the effect of Vanin-1 overexpression on lipid metabolism, we evaluated the circulating lipids in mice fed HFD. Serological analysis revealed that serum levels of TG and TC were significantly decreased in HFD-AAV-Vanin-1 mice compared to control mice (Fig. S5A and S5B). Additionally, we found that livers from HFD-AAV-Vanin-1 mice exhibited reduced steatosis, as evidenced by decreased organ weight, neutral lipid accumulation, and TG content, when compared to HFD-AAV-GFP mice (Fig. S5C—S5F). These findings suggest that mice with BAT-specific overexpression of Vanin-1 were resistant to over-nutrition induced hepatic steatosis and hypertriglyceridemia. Unhealthy expansion of WAT has been associated with hypertrophic white adipocytes, which may result in glucose intolerance and insulin resistance. Given that BAT-specific Vanin-1 overexpression mice showed improved glucose tolerance and insulin sensitivity, we further investigated the secondary effects of BAT Vanin-1 overexpression on WAT. Morphological analyses revealed a decrease in both the volume and weight of sWAT and eWAT (Fig. S5G and S5H). To assess white adipocyte size, we performed H&E staining of sWAT and eWAT in HFD-AAV-GFP or HFD-AAV-Vanin-1 mice. We observed a decrease in adipocyte size in the HFD-AAV-Vanin-1 mice compared to HFD-AAV-GFP mice (Fig. S5I and S5K). Moreover, the number of small-size adipocytes was higher in the HFD-AAV-Vanin-1 group than HFD-AAV-GFP group (Fig. S5J and S5L).

Taken together, these results indicate that BAT-specific Vanin-1 overexpression protects mice from HFD-induced obesity, insulin resistance, hypertriglyceridemia and hepatic steatosis.

3.5. Vanin-1 overexpression alleviates obesity-induced reduction and dysfunction of mitochondrial in mice

Given our data showing that Vanin-1 deficiency reduces mitochondrial respiratory chain activity and disrupts mitochondrial homeostasis in brown adipocytes, we investigated whether Vanin-1 gain-of-function in HFD-AAV-Vanin-1 mice could alleviate HFD-induced BAT whitening. Phenotypically, we observed that the abnormal expansion of BAT induced by HFD was attenuated in mice with AAV-mediated Vanin-1 overexpression (Figure 5A). Consistently, the weight of BAT was remarkably decreased in HFD-AAV-Vanin-1 mice (Figure 5B). Histological analysis revealed that, in contrast to the results described in Figure 2, the cell size of brown adipocytes in HFD mice was reduced in the Vanin-1-overexpressed group (Figure 5C,D). Furthermore, the expression levels of genes related to thermogenesis, both at the RNA and protein level, were increased in Vanin-1-overexpressed mice (Figure 5E, F and Fig. S4F). Based on the thermal damage and abnormal expansion observed in the BAT of Vanin-1$^{-/-}$ mice, we further investigated the effects of Vanin-1 overexpression on the structure and function of mitochondria in BAT from HFD-fed mice. TEM analysis showed that rearing with HFD resulted in the swelling of mitochondria and destruction of the mitochondrial membrane in BAT, but the mitochondria in the BAT of HFD-AAV-Vanin-1 mice exhibited complete structure with increased cristae packing, mitochondrial abundance, and mtDNA copy number (Figure 5G—I). Importantly, increased expression of ETC-related genes indicated that Vanin-1 expression promotes mitochondrial oxidative phosphorylation (Figure 5J, K and Fig. S4F). These results suggest that mice with BAT-specific overexpression of Vanin-1 are resistant to HFD-induced damage to mitochondrial integrity and mass.

3.6. Overexpression of Vanin-1 increases respiratory metabolism in brown adipocytes

To determine whether Vanin-1 affects the thermogenic program in primary adipocytes, we induced the differentiation and maturation of isolated primary brown adipocyte progenitors and treated with adenovirus-expressing Vanin-1 (Ad-Vanin-1) or adenovirus-expressing GFP (Ad-GFP) as a control. The treatment with Ad-Vanin-1 effectively increased the expression of Vanin-1 in the differentiated brown adipocytes (Fig. S6A—S6C). We used a Seahorse XF-24 extracellular flux analyzer to measure various mitochondrial parameters. Our results revealed that basal mitochondrial respiration, maximal mitochondrial respiratory capacity, and ATP production capacity were all increased in the Vanin-1 overexpression group and decreased after in Vanin-1 knockdown group (Figure 6A—D and Fig. S6H—S6K). Additionally, we observed an increase in the number of mitochondria, as measured by MitoTracker, after overexpressing Vanin-1 (Figure 6E). Furthermore, the overexpression of Vanin-1 in primary adipocytes led to a significant upregulation of genes associated with thermogenesis as well as ETC-related genes (Figure 6F,G). Consistently, the protein levels of thermogenesis and ETC-related genes were also elevated in the Ad-Vanin-1 group (Figure 6H and Fig. S6D). These findings suggest that Vanin-1 can enhance metabolic function by improving mitochondrial function, contrary to the observation that Vanin-1 deficiency impairs BAT thermogenesis.

3.7. Cysteamine restores mitochondria function in Vanin-1 null mice

To confirm the regulatory function of Vanin-1 on BAT mitochondrial homeostasis, we used adenovirus to perform Vanin-1 restoring in Vanin-1$^{-/-}$ mice. We also performed TEM of BAT to investigate mitochondrial morphology in the Ad-Vanin-1 mice. Our findings revealed that the mitochondrial cristae morphology was altered in Ad-GFP mice, whereas Vanin-1$^{-/-}$ mice that overexpress vanin-1 exhibited an increase in mitochondrial cristae and a more complete structure (Fig. S7A). Furthermore, mitochondrial abundance and mtDNA copy number also increased in Vanin-1$^{-/-}$ mice after restore with Vanin-1 (Fig. S7B and S7C). In addition, the protein expression levels of ETC-related genes were increased in BAT from Vanin-1$^{-/-}$ mice overexpressing vanin-1 (Fig. S7D and S7E). Collectively, these results suggest that overexpression of vanin-1 in Vanin-1$^{-/-}$ mice can restore the damage to mitochondrial morphology and improve BAT function.

Vanin-1 is a typical pantetheinase that catalyzes the production of cysteamine. Cysteamine has been FDA-approved for the treatment of cystinosis, an inherited autosomal recessive disorder, and has also been evaluated for the treatment of neurodegenerative disorders. After AAV-Vanin-1 administration, we observed an increase in serum levels of cysteamine in mice (Table S3). This finding suggests that the increased cysteamine levels may play a role in alleviating BAT function in HFD mice. To investigate the potential beneficial effects of cysteamine on mitochondria homeostasis in BAT, we administered cysteamine to Vanin-1$^{-/-}$ mice. As shown in Figure 7A, body weight gain in Vanin-1$^{-/-}$ mice were significantly decreased after cysteamine administration. There was no difference in food intake between the two groups of mice under cysteamine administration (Figure 7B). However, the BAT of cysteamine-treated Vanin-1$^{-/-}$ mice appeared browner than that of control mice (Figure 7C). Morphological and histological analyses indicated that the weights of BAT were decreased, while the

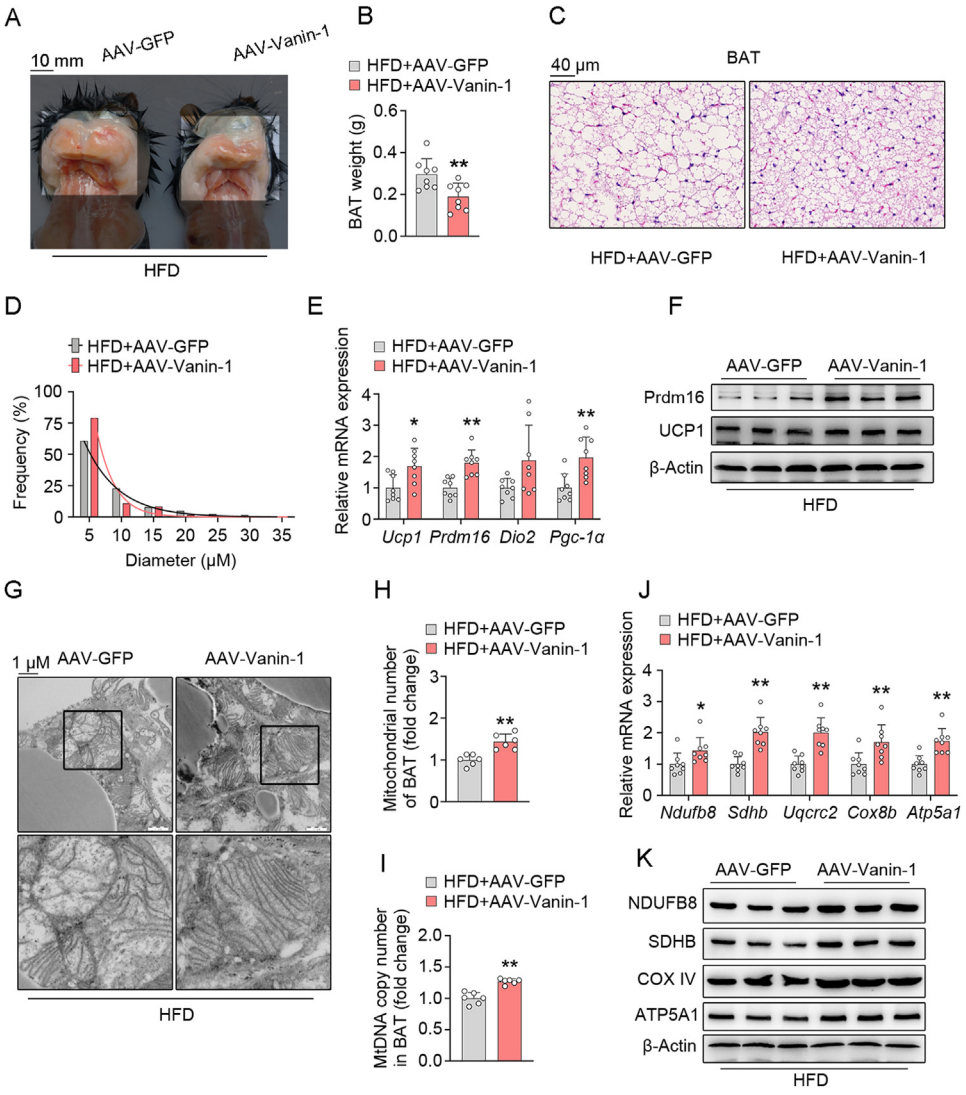

Figure 5: BAT-specific Vanin-1 overexpression contributing to the alleviation of BAT whitening and restoration of mitochondrial morphology in HFD mice
(A) Representative images of BAT from AAV-GFP or AAV-Vanin-1 injection mice fed on HFD for 10 weeks. (B) The weight of BAT from the mice in (A) ($n = 8$). (C) Representative images of H&E staining in BAT from the mice in (A). Scale bar, 40 μm. (D) Distribution of brown adipocyte diameter (μm) in (C). (E) RT-qPCR analysis of thermogenic-related genes mRNA expression in BAT from AAV-GFP or AAV-Vanin-1 injection mice fed on HFD for 10 weeks ($n = 8$) (F) Representative Western blot analysis of Prdm16 and UCP1 protein expression in BAT from AAV-GFP or AAV-Vanin-1 injection mice fed on HFD for 10 weeks ($n = 6$). β-actin was used as a loading control. (G and H) Mitochondrial structures of BAT from AAV-GFP or AAV-Vanin-1 injection mice fed on HFD for 10 weeks. (G) Representative electron microscopy (EM) images of BAT. Black boxes denote magnified areas. Scale bar, 1 μm. (H) Quantification of mitochondrial numbers. Six fields were randomly chosen for each group. (I) mtDNA copy number of BAT from WT and Vanin-1$^{-/-}$ mice ($n = 6$). (J) RT-qPCR analysis of ETC-related genes mRNA expression in BAT from AAV-GFP or AAV-Vanin-1 injection mice fed on HFD for 10 weeks ($n = 8$). (K) Representative western blot analysis of ETC-related genes protein expression in BAT from AAV-GFP or AAV-Vanin-1 injection mice fed on HFD for 10 weeks ($n = 6$). β-actin was used as a loading control. For statistical analysis, unpaired two-tailed Student's *t* tests were performed in (B), (E), (H), (I), and (J). $^{*}p < 0.05$, $^{**}p < 0.01$. All values are presented as the mean ± SD.

number of small-size adipocytes was increased in the cysteamine-treated cohorts, when compared to the control group (Figure 7D—F). We also performed TEM of BAT to investigate mitochondrial morphology in the Vanin-1$^{-/-}$ mice treated with cysteamine. The results showed that mitochondria in Vanin-1$^{-/-}$ mice exhibited altered mitochondrial cristae morphology, whereas those in cysteamine-treated Vanin-1$^{-/-}$ mice showed an increase in mitochondrial cristae and more complete structure (Figure 7G). Furthermore, mitochondrial abundance and mtDNA copy number also increased in Vanin-1$^{-/-}$ mice after treatment with cysteamine (Figure 7H,I). Additionally, the mRNA and protein expression levels of thermogenesis and ETC-related genes were increased in BAT from cysteamine-treated Vanin-1$^{-/-}$ mice (Figure 7J, K and Fig. S8L). These results collectively suggest that cysteamine can recover mitochondrial morphology damage and improve BAT function.

To determine whether cysteamine affects the thermogenic program in primary brown adipocytes, we conducted a 24-hour treatment of primary brown adipocytes with cysteamine. The mitochondrial respiratory capacities calculated as OCR, based on Seahorse XF Analyzer assays, were compared between controls and cysteamine-treated groups. As depicted in Fig. S8A, the respiratory rate in the cysteamine-treated brown adipocytes were significantly higher than that in the control cells. Moreover, the cysteamine-treated adipocytes exhibited an enhanced ability to carry out basal respiration, FCCP-stimulated maximal respiration, and ATP production (Fig. S8B—S8D). By utilizing MitoTracker, we observed an increase in the number of

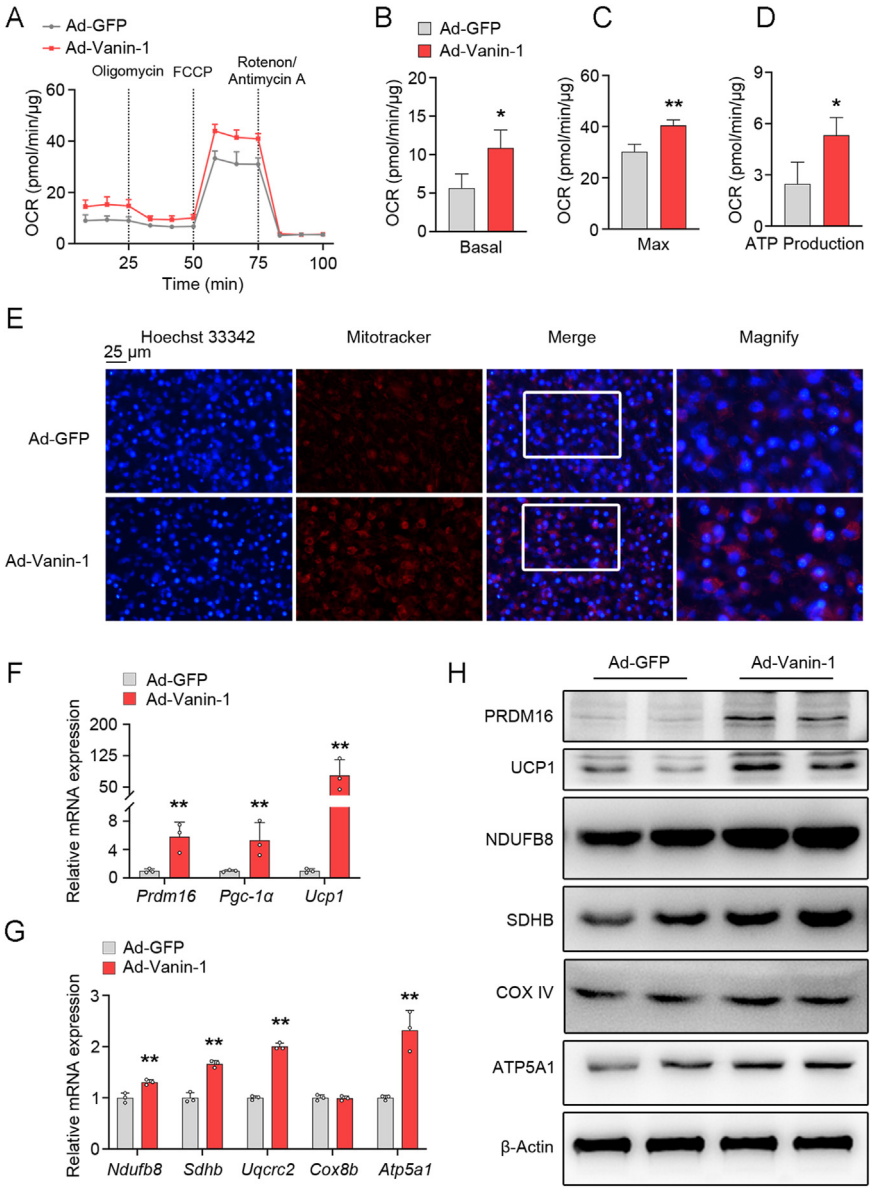

Figure 6: Vanin-1 overexpression induces thermogenesis in brown adipocytes. (A) Representative oxygen consumption rate (OCR) of differentiated primary brown adipocytes infected with Ad-GFP or Ad-Vanin-1, as monitored using a Seahorse XF analyzer. (B) Basal OCR of primary brown adipocytes described in (A). Basal OCR corresponds to baseline OCR minus rotenone/antimycin A-insensitive OCR. (C) Maximal OCR of primary brown adipocytes described in (A). Maximal OCR corresponds to FCCP-induced OCR minus rotenone/antimycin A-insensitive OCR. (D) ATP-linked respiration of primary brown adipocytes described in (A). ATP-linked respiration corresponds to baseline OCR minus Oligomycin-insensitive OCR. (E) Representative images of Mitotracker (Red) and Hoechst 33342 (blue) staining in differentiated primary brown adipocytes infected with Ad-GFP or Ad-Vanin-1. Scale bar, 25 μm. (F and G) RT-qPCR analysis of thermogenic-related genes (F) and ETC-related genes (G) in differentiated primary brown adipocytes infected with Ad-GFP or Ad-Vanin-1 ($n = 3$). (H) Representative western blot analysis of thermogenic-related genes and ETC-related genes protein expression in differentiated primary brown adipocytes infected with Ad-GFP or Ad-Vanin-1 ($n = 3$). β-actin was used as a loading control. For statistical analysis, unpaired two-tailed Student's *t* tests were performed in (B), (C), (D), (F), and (G). $^{*}p < 0.05$, $^{**}p < 0.01$. All values are presented as the mean ± SD.

mitochondria following cysteamine treatment (Fig. S8E). Additionally, in line with in vivo results, the gene expression of both mitochondrial thermogenesis marker genes and ETC complex genes was upregulated in cysteamine-treated brown adipocytes (Fig. S8F—S8K). These findings indicate that cysteamine has the potential to improve metabolic function by enhancing mitochondrial function, which aligns with the observation that Vanin-1overexpression induces BAT thermogenesis. In conclusion, our findings suggest that targeting Vanin-1 could be crucial in regulating BAT function.

4. DISCUSSION

Despite implementing intensive lifestyle changes, the severity of obesity necessitates a more aggressive intervention. Medication plays a crucial role in managing obesity and is categorized into two classical categories: appetite suppressants and pancreatic lipase inhibitors, which limit the absorption of intestinal fat. However, the financial pressures and undesirable side effects (such as mood disorders, cardiovascular disease, and mortality) associated with long medication

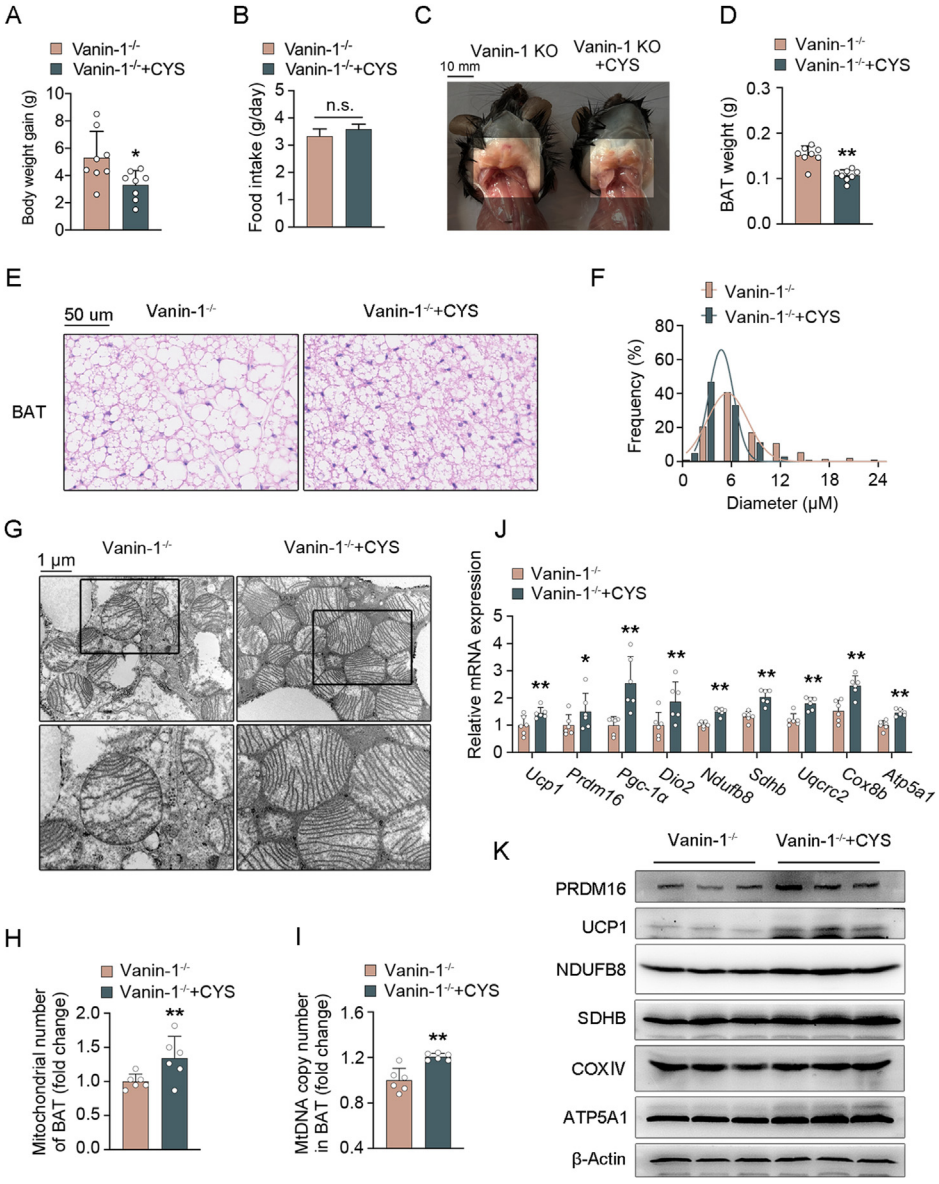

Figure 7: Cysteamine reverses the mitochondrial abnormalities caused by Vanin-1 deficiency in BAT. (A) Body weight gain of Vanin-1$^{-/-}$ mice treated with cysteamine or not for 4 weeks ($n = 8$). (B) Daily food intake of Vanin-1$^{-/-}$ mice treated with cysteamine or not for 4 weeks. (C) Representative images of BAT from Vanin-1$^{-/-}$ mice treated with cysteamine or not for 4 weeks. (D) The weight of BAT from the mice in (C) ($n = 8$). (E) Representative images of H&E staining in BAT from the mice in (C). Scale bar, 50 μm. (F) Distribution of brown adipocyte diameter (μm) in (E). (G and H) Mitochondrial structures of BAT from Vanin-1$^{-/-}$ mice treated with cysteamine or not for 4 weeks. (G) Representative electron microscopy (EM) images of BAT. Black boxes denote magnified areas. Scale bar, 1 μm. (H) Quantification of mitochondrial numbers. Six fields were randomly chosen for each group. (I) mtDNA copy number of BAT from Vanin-1$^{-/-}$ mice treated with cysteamine or not for 4 weeks. ($n = 6$). (J) RT-qPCR analysis of thermogenic-related genes and ETC-related genes in BAT from Vanin-1$^{-/-}$ mice treated with cysteamine or not for 4 weeks. ($n = 6$). (K) Representative Western blot analysis of thermogenic-related genes and ETC-related genes protein expression in BAT from Vanin-1$^{-/-}$ mice treated with cysteamine or not for 4 weeks. β-actin was used as a loading control. For statistical analysis, unpaired two-tailed Student's t tests were performed in (A), (B), (D), (H), (I), and (J). $^{*}p < 0.05$, $^{**}p < 0.01$. All values are presented as the mean ± SD.

cycles can significantly reduce patients' willingness to take medication and diminish the effectiveness of treatment. Given the important role of thermogenic brown adipocytes in maintaining energy balance, increasing the mass or activity of BAT has emerged as an attractive preventive and therapeutic strategy for combating obesity. The whitening of BAT under conditions of obesity and aging exacerbates systemic metabolic disorders.

Here, we investigate the molecular mechanisms underlying BAT whitening in the context of obesity. Our findings reveal the crucial role of Vanin-1 in promoting mitochondrial respiration and thermogenic function in brown adipocytes. Notably, we observe a significant reduction in the expression of Vanin-1 in the BAT of obese mice. Through further experiments, we demonstrate that Vanin-1 deficiency leads to decreased levels of key thermogenic genes and proteins both in vitro and in vivo. Moreover, we also observe that HFD-induced whitening of classical interscapular BAT is more pronounced in Vanin-1$^{-/-}$ mice. On the other hand, overexpression of Vanin-1 in BAT enhances mitochondrial thermogenesis. Importantly, mice with Vanin-1 overexpression in BAT exhibit a higher capacity to maintain body temperature but also show resistance to diet-induced obesity and

metabolic disorders. Furthermore, we find that treatment with cysteamine is able to reverse the blunted mitochondria in the BAT of Vanin-$1^{-/-}$ mice, as evidenced by improvements in mitochondrial structure. Vanin-1, a pantetheinase, plays a key role in catalyzing the hydrolysis of pantetheine into vitamin B5 and cysteamine. Previous clinical and animal experiments have suggested that Vanin-1 is also involved the regulation of metabolic homeostasis. In our previous study, we demonstrated the significance of Vanin-1 in activating lipolysis in WAT [32]. In our current study, we observed a higher expression of Vanin-1 in BAT compared to WAT (Figure 1A). BAT, which contains more mitochondria, is likely responsible for the increased expression of Vanin-1 in this tissue. To confirm this, we conducted Western blot and immunofluorescence analyses, which revealed the mitochondrial localization of Vanin-1, a finding that had not been previously reported. Previous studies conducted by our laboratory and others have demonstrated that serum levels and hepatic expression of Vanin-1 are induced in both obese mice and humans. However, our previous study revealed a significantly reduced expression of Vanin-1 in the WAT of obese mice and humans. In the current study, we also observed a reduced expression of Vanin-1 in the BAT of obese mice (Figure 1B). These findings suggest that changes in Vanin-1 expression in different adipose tissues are consistent in their response to energy signaling.

Obesity in mice has previously been reported to cause BAT hypotrophy, BAT whitening and loss of function. This study provides the first evidence that Vanin-1 deficiency significantly exacerbates BAT whitening in HFD-fed mice, as evidenced by the increased accumulation of enlarged lipid droplets in brown adipocytes, and the associated changes in the expression of BAT and WAT markers. Several transcription factors, such as Rbl1 and Nrip1, suppress thermogenesis by interfering with PGC-1α activity [36]. Rbl1 a tumor suppressor, also plays a key role in adipogenesis and WAT amplification by repressing PGC-1α transcription in white adipocytes. Nrip1 binds to PGC-1α and blocks its transcriptional activity. Silencing of Nrip1 in WAT resulted in browning of adipocytes and enhanced mitochondrial respiration. Therefore, both RBL1 and Nrip1 are considered important regulatory molecules in the transdifferentiation between BAT and WAT. However, no changes in the expression of RBL1 and Nrip1 were detected in the BAT of Vanin-$1^{-/-}$ mice. Similarly, there were no significant changes in the expression of Adiponectin, the classical WAT marker gene. Notably, the expression of these genes was significantly upregulated in Vanin-$1^{-/-}$ mice fed with HFD. Consequently, the downregulation of Vanin-1 is considered to be an important driver in the development of BAT whitening in obesity.

BAT contains a large number of mitochondria for thermogenesis through mitochondrial respiration. Therefore, mitochondria are considered the most important organelles in brown adipocytes, and the homeostasis of mitochondria directly affects the biological function of BAT. Numerous reports have indicated that a phenotypic switch from brown to white-like adipocyte during whitening may result from a decrease in the number and function of mitochondria. Mitochondrial functions such as fatty acid oxidation (FAO), tricarboxylic acid cycle (TCA) cycle, and ETC are essential for UCP1-mediated adaptive thermogenesis in brown adipocytes [37]. Transcriptomic analysis reveals the inhibition of the mitochondrial oxidative phosphorylation pathway in BAT of Vanin-$1^{-/-}$ mice. Additionally, the deletion of Vanin-1 leads to a significant reduction in the expression of ETC complex genes.

Recent independent studies have found a connection between BAT defects and systemic metabolism stress, regardless of their thermogenic function. This connection helps to counteract obesity and insulin resistance. One possible mechanism is the decrease in the expression of ETC complex genes, which can result in mitochondrial disorders and impaired adaptive thermogenesis. On the other hand, two different mouse models (Lkb1BKO and TfamBKO mice) exhibit an imbalance in the ETC proteome but still show reduced adiposity and hepatic lipid accumulation [38]. Supporting these findings, another study demonstrated that deficiency of TRX2, a mitochondrial redox protein that scavenges mtROS, in brown adipocytes disrupts mitochondrial integrity and function [39]. However, this deficiency actually benefits systemic metabolism by reducing HFD-induced adiposity and hepatic steatosis. Given the strong capacity of BAT to clear circulating TGs, increased lipid uptake in BAT may contribute to the metabolic improvement in $Trx2^{BATKO}$ mice. In contrast to previous research, our study found that AAV-mediated Vanin-1 overexpression in BAT significantly reduced HFD-induced adiposity, decreased ectopic fat accumulation in the liver, improved blood metabolic parameters, and enhanced insulin sensitivity. Our results also revealed that Vanin-1 overexpression increases the expression of ETC components, thereby enhancing mitochondrial respiration as evidenced by elevated OCR and upregulated thermogenic gene UCP1. This is consistent with previous studies showing that overexpression of Aifm2 promotes mitochondrial oxidative metabolism and ETC activity in BAT cells [40]. In fact, total deficiency of Aifm2 or its specific deficiency in brown adipose tissue impairs glycolytic capacity, thermogenesis, and cold tolerance, leading to reduced energy expenditure and increased adiposity. Similarly, reducing PGC-1α-mediated mitochondrial biogenesis in brown-adipocyte-specific Irf4 and Hdac3 knockout mice affects the expression of both mtDNA- and nuclear-encoded genes in BAT, resulting in thermogenic defects but without metabolic benefits [41,42]. Remarkably, our results further showed that Vanin-1 overexpression significantly increased ATP-linked respiration in brown adipocytes. Considering the upregulated UCP1 activity and the proton leak respiration, it is reasonable to believe that both UCP1-dependent and -independent thermogenesis are involved in Vanin-1-mediated thermogenesis. Together, our findings strongly suggest that Vanin-1 may serve as a potential therapeutic target for obesity. Additionally, our study highlights the role of BAT mitochondria in regulating systemic metabolism through their thermogenic function.

As an GPI-anchored enzyme, Vanin-1 does not have the ability to directly regulate thermogenic function. However, several studies have demonstrated that the pantetheinase activity of Vanin-1 plays a crucial role in its physiological functions. Our findings indicate that cysteamine effectively improves mitochondrial abnormalities in BAT, enhances the expression of thermogenic and ETC related genes, and promotes respiration in brown adipocytes of Vanin-$1^{-/-}$ mice. Previous research has shown diverse functions of cysteamine and its disulfide form, cystamine [43,44]. Recent studies have demonstrated that cysteamine inhibits the glycolytic pathway and reduces lactate release in aggressive soft tissue sarcomas. Furthermore, cysteamine and cystamine have been found to prevent mitochondrial depolarization induced by 3-NP [45]. Since mitochondria are a major source of intracellular free radicals, cystamine and cysteamine can protect against 3-NP-induced mitochondrial dysfunction in a glutathione-dependent manner. In fact, cysteamine bitartrate has been shown to alleviate oxidative stress in primary mitochondrial respiratory chain diseases, leading to improved cellular viability and overall organismal health [46]. Notably, our study reveals that cysteamine significantly induces mitochondrial respiration and thermogenesis in primary brown adipocytes even under basal conditions without oxidative stress. Therefore, it is important to investigate the direct regulation of mitochondrial proteins by cysteamine, which has the ability to cleave sulphhydryl bonds within proteins.

Considering the germline deletion of Vanin-1, it is important to acknowledge that the impact of Vanin-1 deficiency on BAT dysfunction

might be influenced by a maladaptive systemic response from other tissues. Additionally, our findings indicate that Vanin-1 is localized in mitochondria. However, further investigation is necessary to fully understand the exact biological significance of this observation. The selective cell-specific localization of Vanin-1 in mitochondria remains unclear and requires additional analysis.

5. CONCLUSIONS

Taken together, our study highlights the crucial role of Vanin-1 in maintaining the health of brown adipose tissue (BAT). We emphasize the significance of Vanin-1-mediated mitochondrial homeostasis in combating obesity. Furthermore, our research provides initial evidence supporting the impact of cysteamine on energy expenditure.

FUNDING

This work was supported by grants from the National Natural Science Foundation of China (92057112 and 31771298), National Key R&D Program of China (2021YFF0702000), the Project of State Key Laboratory of Natural Medicines, China Pharmaceutical University (SKLNMZZ202214), Traditional Chinese Medicine Science Project of Shandong Province (M-2023093), Key Project of Natural Science Foundation ,Xinjiang Uygur Autonomous Region (2023D01D09).

CREDIT AUTHORSHIP CONTRIBUTION STATEMENT

Chen Sun: Writing — review & editing, Writing — original draft, Supervision, Software, Resources, Project administration, Methodology, Formal analysis, Data curation, Conceptualization. **Jiaqi Liang:** Writing — review & editing, Writing — original draft, Resources, Methodology, Formal analysis, Data curation. **Jia Zheng:** Data curation. **Shuyu Mao:** Project administration, Data curation. **Siyu Chen:** Resources, Methodology, Conceptualization. **Ainiwaer Aikemu:** Resources, Funding acquisition, Conceptualization. **Chang Liu:** Writing — review & editing, Writing — original draft, Funding acquisition, Conceptualization.

ACKNOWLEDGMENTS

Not applicable.

DECLARATION OF COMPETING INTEREST

The authors declare that they have no known competing financial interests or personal relationships that could have appeared to influence the work reported in this paper.

DATA AVAILABILITY

Data will be made available on request.

APPENDIX A. SUPPLEMENTARY DATA

Supplementary data to this article can be found online at https://doi.org/10.1016/j.molmet.2024.101884.

REFERENCES

[1] Kushner RF, Calanna S, Davies M, Dicker D, Garvey WT, Goldman B, et al. Semaglutide 2.4 mg for the treatment of obesity: key elements of the STEP trials 1 to 5. Obesity 2020;28:1050—61.
[2] Loos RJF, Yeo GSH. The genetics of obesity: from discovery to biology. Nat Rev Genet 2022;23:120—33.
[3] Lin X, Li H. Obesity: epidemiology, pathophysiology, and therapeutics. Front Endocrinol 2021;12:706978.
[4] Muller TD, Bluher M, Tschop MH, DiMarchi RD. Anti-obesity drug discovery: advances and challenges. Nat Rev Drug Discov 2022;21:201—23.
[5] Harwood Jr HJ. The adipocyte as an endocrine organ in the regulation of metabolic homeostasis. Neuropharmacology 2012;63:57—75.
[6] Herz CT, Kiefer FW. Adipose tissue browning in mice and humans. J Endocrinol 2019;241:R97—109.
[7] van Marken Lichtenbelt WD, Schrauwen P. Implications of nonshivering thermogenesis for energy balance regulation in humans. Am J Physiol Regul Integr Comp Physiol 2011;301:R285—96.
[8] Carpentier AC, Blondin DP, Haman F, Richard D. Brown adipose tissue — a translational perspective. Endocr Rev 2023;44:143—92.
[9] Scheel AK, Espelage L, Chadt A. Many ways to Rome: exercise, cold exposure and diet-do they all affect BAT activation and WAT browning in the same manner? Int J Mol Sci 2022;23.
[10] Lee P, Swarbrick MM, Ho KK. Brown adipose tissue in adult humans: a metabolic renaissance. Endocr Rev 2013;34:413—38.
[11] Symonds ME, Aldiss P, Pope M, Budge H. Recent advances in our understanding of brown and beige adipose tissue: the good fat that keeps you healthy. F1000 Res 2018;7.
[12] Sharma BK, Patil M, Satyanarayana A. Negative regulators of brown adipose tissue (BAT)-mediated thermogenesis. J Cell Physiol 2014;229:1901—7.
[13] Chouchani ET, Kazak L, Spiegelman BM. New advances in adaptive thermogenesis: UCP1 and beyond. Cell Metab 2019;29:27—37.
[14] Roesler A, Kazak L. UCP1-independent thermogenesis. Biochem J 2020;477:709—25.
[15] Kazak L, Cohen P. Creatine metabolism: energy homeostasis, immunity and cancer biology. Nat Rev Endocrinol 2020;16:421—36.
[16] Shimizu I, Walsh K. The whitening of brown fat and its implications for weight management in obesity. Curr Obes Rep 2015;4:224—9.
[17] Gao P, Jiang Y, Wu H, Sun F, Li Y, He H, et al. Inhibition of mitochondrial calcium overload by SIRT3 prevents obesity- or age-related whitening of brown adipose tissue. Diabetes 2020;69:165—80.
[18] Ziqubu K, Dludla PV, Mthembu SXH, Nkambule BB, Mabhida SE, Jack BU, et al. An insight into brown/beige adipose tissue whitening, a metabolic complication of obesity with the multifactorial origin. Front Endocrinol 2023;14:1114767.
[19] Shimizu I, Aprahamian T, Kikuchi R, Shimizu A, Papanicolaou KN, MacLauchlan S, et al. Vascular rarefaction mediates whitening of brown fat in obesity. J Clin Invest 2014;124:2099—112.
[20] Rangel-Azevedo C, Santana-Oliveira DA, Miranda CS, Martins FF, Mandarim-de-Lacerda CA, Souza-Mello V. Progressive brown adipocyte dysfunction: whitening and impaired nonshivering thermogenesis as long-term obesity complications. J Nutr Biochem 2022;105:109002.
[21] Tanaka Y, Nagoshi T, Takahashi H, Oi Y, Yoshii A, Kimura H, et al. URAT1-selective inhibition ameliorates insulin resistance by attenuating diet-induced hepatic steatosis and brown adipose tissue whitening in mice. Mol Metab 2022;55:101411.
[22] Bartucci R, Salvati A, Olinga P, Boersma YL. Vanin 1: its physiological function and role in diseases. Int J Mol Sci 2019;20.
[23] Nitto T, Onodera K. Linkage between coenzyme a metabolism and inflammation: roles of pantetheinase. J Pharmacol Sci 2013;123:1—8.
[24] Atallah C, Charcosset C, Greige-Gerges H. Challenges for cysteamine stabilization, quantification, and biological effects improvement. J Pharm Anal 2020;10:499—516.
[25] Paul BD, Snyder SH. Therapeutic applications of cysteamine and cystamine in neurodegenerative and neuropsychiatric diseases. Front Neurol 2019;10:1315.

[26] Wood PL, Khan MA, Moskal JR. Cellular thiol pools are responsible for sequestration of cytotoxic reactive aldehydes: central role of free cysteine and cysteamine. Brain Res 2007;1158:158—63.
[27] Wilmer MJ, Kluijtmans LA, van der Velden TJ, Willems PH, Scheffer PG, Masereeuw R, et al. Cysteamine restores glutathione redox status in cultured cystinotic proximal tubular epithelial cells. Biochim Biophys Acta 2011;1812:643—51.
[28] Jeitner TM, Lawrence DA. Mechanisms for the cytotoxicity of cysteamine. Toxicol Sci 2001;63:57—64.
[29] Pitari G, Malergue F, Martin F, Philippe JM, Massucci MT, Chabret C, et al. Pantetheinase activity of membrane-bound Vanin-1: lack of free cysteamine in tissues of Vanin-1 deficient mice. FEBS Lett 2000;483:149—54.
[30] van Diepen JA, Jansen PA, Ballak DB, Hijmans A, Hooiveld GJ, Rommelaere S, et al. PPAR-alpha dependent regulation of vanin-1 mediates hepatic lipid metabolism. J Hepatol 2014;61:366—72.
[31] Chen S, Zhang W, Tang C, Tang X, Liu L, Liu C. Vanin-1 is a key activator for hepatic gluconeogenesis. Diabetes 2014;63:2073—85.
[32] Chen S, Zhang W, Sun C, Song M, Liu S, Xu M, et al. Systemic nanoparticle-mediated delivery of pantetheinase vanin-1 regulates lipolysis and adiposity in abdominal white adipose tissue. Adv Sci 2020;7:2000542.
[33] Giessner C, Millet V, Mostert KJ, Gensollen T, Vu Manh TP, Garibal M, et al. Vnn1 pantetheinase limits the Warburg effect and sarcoma growth by rescuing mitochondrial activity. Life Sci Allian 2018;1:e201800073.
[34] Kutiyanawalla A, Terry Jr AV, Pillai A. Cysteamine attenuates the decreases in TrkB protein levels and the anxiety/depression-like behaviors in mice induced by corticosterone treatment. PLoS One 2011;6:e26153.
[35] Deng J, Guo Y, Yuan F, Chen S, Yin H, Jiang X, et al. Autophagy inhibition prevents glucocorticoid-increased adiposity via suppressing BAT whitening. Autophagy 2020;16:451—65.
[36] Harms M, Seale P. Brown and beige fat: development, function and therapeutic potential. Nat Med 2013;19:1252—63.
[37] Calderon-Dominguez M, Mir JF, Fucho R, Weber M, Serra D, Herrero L. Fatty acid metabolism and the basis of brown adipose tissue function. Adipocyte 2016;5:98—118.
[38] Masand R, Paulo E, Wu D, Wang Y, Swaney DL, Jimenez-Morales D, et al. Proteome imbalance of mitochondrial electron transport chain in brown adipocytes leads to metabolic benefits. Cell Metab 2018;27:616—29. e614.
[39] Huang Y, Zhou JH, Zhang H, Canfran-Duque A, Singh AK, Perry RJ, et al. Brown adipose TRX2 deficiency activates mtDNA-NLRP3 to impair thermogenesis and protect against diet-induced insulin resistance. J Clin Invest 2022;132.
[40] Nguyen HP, Yi D, Lin F, Viscarra JA, Tabuchi C, Ngo K, et al. Aifm2, a NADH oxidase, supports robust glycolysis and is required for cold- and diet-induced thermogenesis. Mol Cell 2020;77:600—617 e604.
[41] Emmett MJ, Lim HW, Jager J, Richter HJ, Adlanmerini M, Peed LC, et al. Histone deacetylase 3 prepares brown adipose tissue for acute thermogenic challenge. Nature 2017;546:544—8.
[42] Kong X, Banks A, Liu T, Kazak L, Rao RR, Cohen P, et al. IRF4 is a key thermogenic transcriptional partner of PGC-1 alpha. Cell 2014;158:69—83.
[43] Kaplan WD, Lyon MF. Failure of mercaptoethylamine to protect against the mutagenic effects of radiation. I. Experiments with *Drosophila*. Science 1953;118:776—7.
[44] Min B, Chung KC. New insight into transglutaminase 2 and link to neurodegenerative diseases. BMB Rep 2018;51:5—13.
[45] Mao Z, Choo YS, Lesort M. Cystamine and cysteamine prevent 3-NP-induced mitochondrial depolarization of Huntington's disease knock-in striatal cells. Eur J Neurosci 2006;23:1701—10.
[46] Guha S, Konkwo C, Lavorato M, Mathew ND, Peng M, Ostrovsky J, et al. Preclinical evaluation of cysteamine bitartrate as a therapeutic agent for mitochondrial respiratory chain disease. Hum Mol Genet 2019;28:1837—52.

